

# Analysis and Modelling of High Frequency Effects on Synchronous Generator's Armature Conductors

Quadir H. Quadir  
Power Electronics, Machines and  
Control Research Group  
University of Nottingham  
Nottingham, UK  
syed.quadri@nottingham.ac.uk

Stefano Nuzzo  
Department of Engineering "Enzo  
Ferrari"  
University of Modena and Reggio  
Emilia  
Modena, Italy  
stefano.nuzzo@unimore.it

Chris Gerada  
Power Electronics, Machines and  
Control Research Group  
University of Nottingham  
Nottingham, UK  
chris.gerada@nottingham.ac.uk

Michael Galea  
Key Laboratory of More Electric  
Aircraft Technology of Zhejiang  
Province  
Ningbo, China  
michael.galea@nottingham.edu.cn

**Abstract**—This paper investigates the accuracy of the subdomain modelling technique for high frequency copper loss calculation in stator windings of synchronous generators. The methodology's accuracy is studied at a slot level up to 10 kHz against FE model with realistic conductor dimensions. The analysis demonstrates that improper conductor area representation and eddy current reaction negligence causes increasing error with increasing frequencies. A modified subdomain model is then proposed to address these challenges which has proven to show a good match with a corresponding FE model.

**Keywords**— Copper loss, eddy current, high frequency, subdomain modelling, synchronous generators

## I. INTRODUCTION

High-frequency (HF) copper loss in the windings of electrical machines has always been an overlooked design aspect, especially for low to medium power range applications. However, with the advent and ever increasing development of power electronic technologies and high speed applications, these losses are becoming ever-more important. Therefore, to ensure an appropriate overall system efficiency, they cannot be neglected anymore [1].

The increasing use of power converters for efficient electrical conditioning and variable speed electrical drives are leading to a higher harmonic content in the power systems due to the switching frequency components inherently introduced by power electronic devices [2]. These harmonic contents are even higher in remote industrial power systems where the percentage of linear loads is not enough to overshadow the non-linear loads [3]. In such systems, the HF current components can result in non-uniform current densities within the armature windings of machines, leading to increased copper losses and reduced efficiency and durability. Despite the above mentioned drawbacks, power electronic capabilities are enabling their wide implementation in generation systems, such as in applications of direct drive variable speed generators [4, 5] and high-power DC supplies [6]. Furthermore, current researches are looking in to reducing the manufacturing cost of synchronous generators (SGs) [7] by replacing its complex design with power electronic modules that improve supply power quality [8-10] and transient behaviour [11]. Such power electronic applications would have even a more direct impact on the SG's armature windings when they are directly connected to its terminals. This enforces the SG manufacturers and designers to analyse more

in detail the effects of these ever-increasing HF harmonics [12] to maintain their products within the stringent standard regulations [13, 14]. To do so, very accurate numerical techniques, such as the finite-element (FE) method, can be employed. However, it is unsuitable for everyday design purposes as it requires a very dense mesh within the slots for reliable results which makes them computationally very expensive, time-consuming and inflexible.

A convenient alternative is subdomain (SD) modelling which is directly based on Maxwell's equations. The SD modelling technique has demonstrated good accuracy in calculating flux, torque, back electromotive force and permanent magnet (PM) losses in PM machines [15, 16]. It has also been used to calculate the eddy currents induced in the rotor bars of squirrel-cage induction machines [17] and in the stator slot windings of PM machines [18, 19]. When used for determining the eddy current loss in slot windings, the conductors are usually modelled by sectionalising the slot domain radially and circumferentially to represent round conductors [18], or only circumferentially to represent vertical conductor winding [19]. This limits the analysis to an ideal 100% slot fill factor which is never achieved in electrical machines. This inherent assumption leads to consider a higher conductor area than that of the actual machine which may cause error in eddy current loss at higher frequencies. SD models are usually validated against FE models having similar 100% slot fill factor and have never been validated or analysed above 1 kHz. Therefore, there is a need to consider this factor in the SD model for HF copper loss and validate it against platforms having realistic conductor dimensions.

This paper addresses the above challenges in the following steps:

- The traditional SD modelling technique (with the inherent assumption of 100% fill factor) is recalled, implemented and analysed against a purposely built FE model.
- An improved SD model which takes into account the "real" slot fill factor of the machine windings is proposed for the calculation of HF copper loss.
- The proposed SD model is validated against FE model with actual conductor dimensions.

## II. TRADITIONAL SUBDOMAIN MODELLING TECHNIQUE

A single slot is considered for SD modelling to exclusively analyse the accuracy of the eddy current loss calculation of the

---

This work was partly supported by the Natural Science Foundation of China with project code 51850410515.

This work has also been supported from the University of Nottingham Propulsion Futures Beacon through Grant PF042.

TABLE I. SYNCHRONOUS GENERATOR SPECIFICATIONS

Parameters	Quantity
Rated power	72.5 kVA
Rated phase terminal voltage	230 V
Frequency	50 Hz
Number of poles	4
Number of slots	48
Stator skew angle	1 slot pitch
Coil pitch	2/3
Slot winding layers	2
Number of conductors per layer	48
Armature phase parallel paths	2

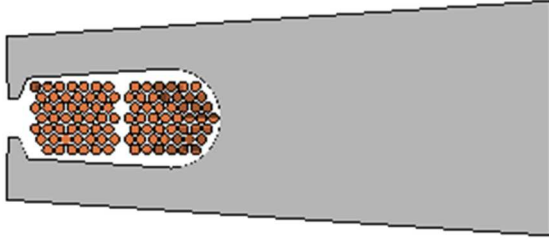


Fig. 1. Slot segment drawing of the considered SG.

winding in a semi-closed slot. The slot dimensions and winding configuration considered for the analysis are based on a 72.5 kVA SG, whose major features are given in TABLE I. A 2-D cross-section of the slot is shown in Fig. 1. The results from the traditional SD model are compared to those obtained through the FE model of a slot with realistic conductor dimensions to check the validity of assuming the whole slot SD as a conducting material.

#### A. Magnetic Vector Potential

The SD model, as classically described in literature, is based on the following assumptions:

- The stator and rotor core materials are infinitely permeable, meaning that the relevant m.m.f. drop can be neglected with respect to that of the machine parts which consist of air.
- The rotor and stator laminations feature zero electric conductivity, which means that the eddy currents can be assumed negligible for the sake of this study.
- A 2-D approximation of the field map is considered, thus neglecting the phenomena occurring at the end regions of the considered SG.

The non-iron area shown in Fig. 2 is divided in to the following 3 subdomains:

- The slot area, where the active sides of the machine coils are physically located (region I in Fig. 2).
- The slot-opening area (region II in Fig. 2).
- The main air-gap (region III in Fig. 2).

The annotations shown in Fig. 2 will be used throughout the paper to define the dimensions. By comparing between the real slot cross-section in Fig. 1 and that shown in Fig. 2, it can be observed that the latter has been slightly altered so that its

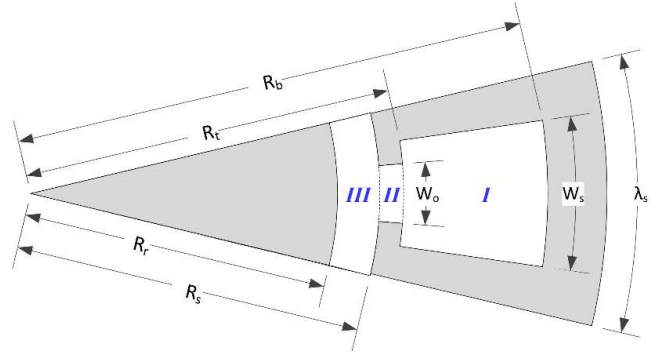


Fig. 2. Subdomain modelling regions I, II, III with dimensions annotations.

boundaries could easily be defined by polar coordinates for modelling. However the area, the average width and depth of the slot are kept equal to the actual slot.

The magnetic vector potential  $A$  in space for each mentioned SD is mathematically defined by (1), where  $\mu$  is the magnetic permeability of the SD material and  $J$  is the current density in the SD. The expanded form of (1) is shown in polar coordinates in (2), having defined  $r$  and  $\theta$  as the radial and tangential coordinates respectively.

$$\nabla^2 A = -\mu J \quad (1)$$

$$\frac{\partial^2 A}{\partial r^2} + \frac{1}{r} \frac{\partial A}{\partial r} + \frac{1}{r^2} \frac{\partial^2 A}{\partial \theta^2} = -\mu J \quad (2)$$

According to the assumption relative to the 2-D approximation of the field map, the vectors  $J$  and  $A$  will always be perpendicular to the plane of the laminations. Considering that the flux density vector  $B$  and magnetic vector potential are related by (3), the radial and circumferential components  $B_r$  and  $B_\theta$  of the flux density can be defined separately as in (4) and (5), respectively.

$$\nabla \times A = B \quad (3)$$

$$B_r = \frac{1}{r} \frac{\partial A}{\partial \theta} \quad (4)$$

$$B_\theta = -\frac{\partial A}{\partial r} \quad (5)$$

Applying and solving (2) at each SD with the imposition of appropriate boundary conditions defined using (4) and (5), the magnetic vector potential solution for each SD can be determined.

The assumption of infinite permeability of iron leads to the following boundary conditions for the slot SD.

- The radial flux density in the slot at the boundaries  $\theta = \pm W_s/2$  is zero, as seen in (6).
- The circumferential flux density in the slot at the boundary  $r = R_b$  is zero, as written in (7).

$$\left. \frac{1}{r} \frac{\partial A_r}{\partial \theta} \right|_{\theta = \pm W_s/2} = 0 \quad (6)$$

$$\left. -\frac{\partial A_r}{\partial r} \right|_{r=R_b} = 0 \quad (7)$$

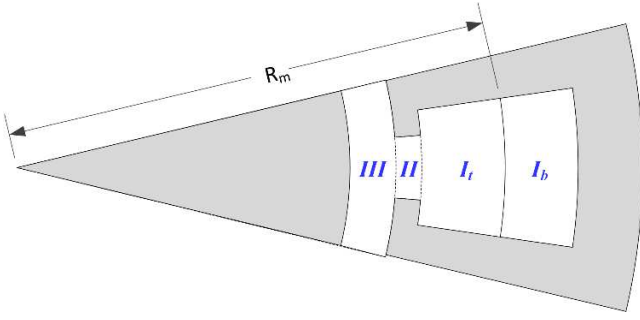


Fig. 3. Slot division to 2 subdomains to represent double layer windings.

As the considered SG armature winding is characterized by a double layer layout, the slot area SD is further divided in to two SDs along the radial direction, namely  $I_t$  and  $I_b$  in Fig. 3. This further separation is necessary to impose different phase currents on the two-layer windings.

Having imposed the conditions (6) and (7), (2) can be solved leading to the expressions (8) and (9), which represent the magnetic vector potential solutions for the bottom ( $A_{Ib}$ ) and top layer ( $A_{It}$ ), respectively [16].  $J_b$  and  $J_t$  represent the current density at the bottom and top layer respectively and the value of  $\alpha_n$  is expressed in (10).

$$A_{Ib} = C_{Ib} + \frac{\mu_o J_b}{4} (2R_b^2 \ln(r) - r^2) + \sum_{n=1}^{\infty} G_{Ib} \left[ \left( \frac{R_t}{R_b} \right)^{\alpha_n} \left( \frac{r}{R_b} \right)^{\alpha_n} + \left( \frac{r}{R_t} \right)^{-\alpha_n} \right] \cos \left[ \alpha_n \left( \theta + \frac{W_s}{2} \right) \right] \quad (8)$$

$$A_{It} = C_{It} + \frac{\mu_o J_t}{2} \left( R_m^2 \ln(r) - \frac{r^2}{2} \right) + \frac{\mu_o J_b}{2} (R_b^2 - R_m^2) \ln(r) + \sum_{n=1}^{\infty} G_{It} \left[ \left( \frac{R_t}{R_b} \right)^{\alpha_n} \left( \frac{r}{R_b} \right)^{\alpha_n} + \left( \frac{r}{R_t} \right)^{-\alpha_n} \right] \cos \left[ \alpha_n \left( \theta + \frac{W_s}{2} \right) \right] \quad (9)$$

$$\alpha_n = \frac{n\pi}{W_s} \quad (10)$$

Similarly, solving (2) for the slot-opening SD using the boundary condition (11) gives the magnetic vector potential of the slot-opening  $A_{II}$  as shown in (12), where  $\beta_m$  is defined as in (13).

$$\frac{1}{r} \frac{\partial A_{II}}{\partial \theta} \Big|_{\theta=\pm W_o/2} = 0 \quad (11)$$

$$A_{II} = C_{II} + D_{II} \ln(r) + \sum_{m=1}^{\infty} \left[ F_{II} \left( \frac{r}{R_t} \right)^{\beta_m} + G_{II} \left( \frac{r}{R_s} \right)^{-\beta_m} \right] \cos \left[ \beta_m \left( \theta + \frac{W_o}{2} \right) \right] \quad (12)$$

$$\beta_m = \frac{m\pi}{W_o} \quad (13)$$

The last SD to be solved represents the air-gap layer. Considering that the rotor is immediately adjacent to this SD, the relevant boundary condition at  $r=R_r$ , can be imposed as in (14). The other boundary condition is the zero circumferential flux density at  $\theta = \pm \lambda_s/2$ , as given in (15). The latter is adopted

considering that the corresponding FE model (described in detail in the next section) assumes the same boundary condition, thus ensuring a fair comparison between results.

$$-\frac{\partial A_{III}}{\partial r} \Big|_{r=R_r} = 0 \quad (14)$$

$$-\frac{\partial A_{III}}{\partial r} \Big|_{\theta=\pm \lambda_s/2} = 0 \quad (15)$$

Considering the conditions (14) and (15), the solution  $A_{III}$  of (2) for the air-gap SD can be expressed as in (16), where the value of  $\delta_k$  can be defined via (17).

$$A_{III} = \sum_{k=1}^{\infty} C_{III} \left[ \left( \frac{r}{R_s} \right)^{\delta_k} + \left( \frac{R_r}{R_s} \right)^{\delta_k} \left( \frac{r}{R_r} \right)^{-\delta_k} \right] \sin \left[ \delta_k \left( \theta + \frac{\lambda_s}{2} \right) \right] \quad (16)$$

$$\delta_k = \frac{k\pi}{\lambda_s} \quad (17)$$

The values of the unknown constants  $C_{Ib}$ ,  $G_{Ib}$ ,  $C_{It}$ ,  $G_{It}$ ,  $C_{II}$ ,  $D_{II}$ ,  $F_{II}$ ,  $G_{II}$  and  $C_{III}$  in (8), (9), (12) and (16) are determined by considering that the values of the magnetic vector potential and the flux density of two neighbouring SDs are equal at the interface between them [16].

The induced eddy current distribution within each conductor can be calculated using the magnetic vector potential solution obtained for the slot SD. In order to model the 96 conductors of the considered SG slot (48 conductors per layer – see TABLE I), the slot is radially and circumferentially divided in 96 regions with each region representing a conductor. Fig. 4 illustrates the conductors' cross-sections after this further subdivision.

The induced eddy current density can be determined by using (18), which is derived from Maxwell's equations. In (18),  $J_e$  is the induced eddy current density,  $\sigma$  is the conductivity of the conductor material (i.e. standard copper) and  $C$  is a time-dependent parameter which ensures that the total current in a conductor is always equal to the excitation current only (i.e. the integral sum of the eddy current in a conductor should always be equal to zero). This concept is represented by (19), where  $r_{c1}$  and  $r_{c2}$  are the lower and upper radial limits of the equivalent conductors (see Fig. 4), whilst  $\theta_{c1}$  and  $\theta_{c2}$  are the angles defining the conductor's edges along the tangential direction.

$$J_e = -\sigma \frac{\partial A_I}{\partial t} + C \quad (18)$$

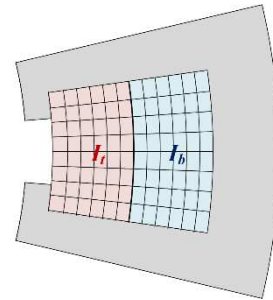


Fig. 4. Slot's radial and circumferential division to represent conductors.

$$\int_{r_{c1}}^{r_{c2}} \int_{\theta_{c1}}^{\theta_{c2}} J_e(r, \theta) r d\theta dr = 0 \quad (19)$$

By substituting in (19) the expression found for  $J_e$  in (18), the constant  $C$  is derived as shown in (20). This allows to obtain the solution for  $J_e$  (see (18)). The total power loss  $P$  in the slot conductors can then be obtained by solving (21), where  $J_c$  is the current density produced by the effective current supplied by the generator and  $l$  is the axial length of the active sides of the slot conductors.

$$C = \frac{2\sigma}{(r_{c2}^2 - r_{c1}^2)(\theta_{c2} - \theta_{c1})} \int_{r_{c1}}^{r_{c2}} \int_{\theta_{c1}}^{\theta_{c2}} \frac{\partial A_l}{\partial t} r d\theta dr \quad (20)$$

$$P = \frac{l}{\sigma} \int_{r_{c1}}^{r_{c2}} \int_{\theta_{c1}}^{\theta_{c2}} (J_e + J_c)^2 r d\theta dr \quad (21)$$

### III. INVESTIGATION OF TRADITIONAL SD MODELLING TECHNIQUE

This section aims at validating the traditional SD modelling solutions derived in Section II against 2-D FE models of the considered SG's single-slot section. To account for the HF effects in the conductors, these have been individually modelled as solid components in the FE model. A number of single-slot FE models have been implemented to investigate the accuracy of the SD model. The main features of these different models are listed below:

- FE model of the actual SG with round conductors and actual slot shape, as shown in Fig. 5(a).
- FE model with round conductors but with the simplified slot shape, as described in Section II.B (see Fig. 5(b)). This is needed to understand how the modified slot shape affects the results.
- FE model with simplified slot shape and square-like conductors (100% fill factor) having 12 radial and 8 circumferential layers (see Fig. 5(c)). This is developed to have the same slot and conductor dimensions as assumed in the SD model (see Fig. 4).
- FE model with simplified slot shape and square-like conductor shape (100% fill factor) having 16 radial layers and 6 circumferential layers (see Fig. 5(d)), to investigate the effects of the conductor arrangement as compared to the SD model.

When modelling the conductors in a SD model, there is no definite rule on the selection of radial and circumferential layers of conductors arranged in a slot. This is usually chosen to be somewhat reflective of the actual machine. For the SG at hand, there are two possible conductor arrangements that

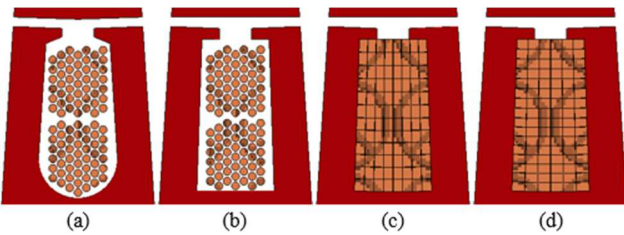


Fig. 5. 2-D FE single-slot models: (a) actual SG conductors arrangement; (b) simplified slot geometry with round conductors; simplified slot and conductor geometry with: (c) 12x8 elements and (d) 16x6 elements.

can be considered, which are shown in Fig. 5(c) and Fig. 5(d). Therefore, FE models with both the conductor arrangements are considered to study their effect on the accuracy. This was done because the selection of the radial and circumferential divisions of the slot for conductors' representation would change the radial and circumferential thickness of the conductors. Therefore, it can have an effect on the HF copper loss calculation. A comparative analysis between these two models would help in the verification of this hypothesis.

In both SD and FE models, the windings have been excited with a sinusoidal current of 1A amplitude, at any considered excitation frequency. The copper loss is thus evaluated at step frequency of 1 kHz up to 10 kHz. Since in the considered alternator, the two winding layers host coils always belonging to different phases (due to the 2/3 coil pitch arrangement) having a 120° electrical phase shift at fundamental frequency, the sinusoidal currents of the winding layers have been separated by the same time shift in the FE simulations. To be coherent with the FE models of Fig. 5(c) and Fig. 5(d), the SD model has been run considering the same conductor arrangements, consisting of having 12x8 and 18x6 layers.

The comparisons between the copper losses calculated via SD and FE models are shown in Fig. 6. Observations from this comparative study are discussed in the next sub-sections.

#### A. Effect of slot shape modification

The comparison between the FE model having the actual slot and conductors shape (green dots) and the FE model with modified slot shape (green crosses) shows an excellent match between results. It can be then safely concluded that the slot shape modification will not affect the SD modelling results, as long as the mean width and area of the slot is maintained.

#### B. Effect of the eddy current reaction

At HFs, the SD models tend to overestimate the copper loss calculation when compared to their respective FE counterparts. The higher copper loss in the SD modelling is due to the fact that at higher frequencies, higher eddy current densities are observed on the sides of the conductor as illustrated in Fig. 7 by dots and crosses. This effect is evermore prominent with the increase of the excitation frequency. These induced eddy currents densities then become high enough to produce flux around it that is capable to oppose the change in leakage flux (see Fig. 7). This is called eddy current reaction. Therefore, the net leakage flux inducing eddy currents in the slot gets reduced by this phenomenon, thus lowering the copper loss. Considering that the diameter of the

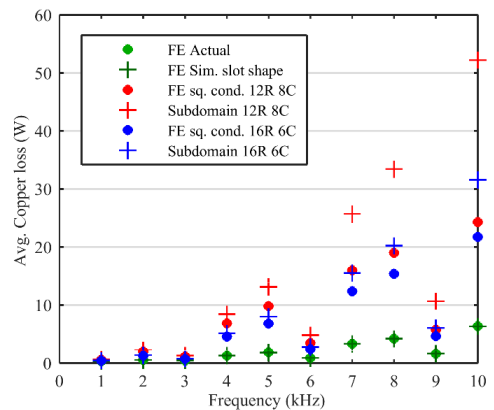


Fig. 6. Average copper loss vs frequency: comparison between SD and FE models.

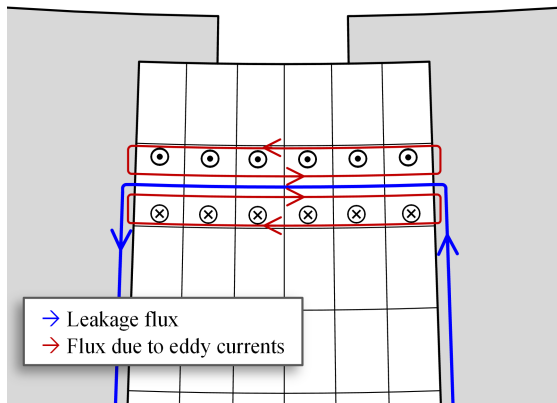


Fig. 7. Eddy current reaction: flux produced by eddy currents opposes the change in leakage flux.

round conductors is very small, the SD model ignores the eddy current reaction and calculates the induced eddy currents based on the leakage flux produced solely by the excitation current. On the contrary, the FE model does consider this phenomenon. Hence, the SD model overestimates the copper loss when the eddy current reaction effect becomes prominent at HF.

Another important aspect to notice in Fig. 6 is that the copper loss is low at the integer multiples of the third harmonics. This is because the currents in the two phases are in-phase at these frequencies and are travelling in the opposite directions in the slot. Therefore, the net leakage flux inducing the eddy currents is very low.

#### C. Effect of 100% fill factor

When comparing the FE models with 100% fill factor (red and blue dots) against the FE model of the actual slot (green dots), it can be noticed that the error increase with the increasing frequency. This indicates that even including the eddy current reaction effect in the current SD model will not represent the copper loss in the actual slot due to the discrepancy in the conductor dimensions. Since the FE models with 100% fill factor have higher conductor thickness than that of the real machine's conductors, the induced eddy current calculation over the extended area of the conductors overestimates the copper loss. This overestimation increases with frequency as the induced eddy current density increases over the edges of the conductors.

#### D. Effect of the conductor arrangement

The comparison between the different conductor arrangements show that the selection of the number of radial and circumferential layers of conductors is also an important factor in the 100% fill factor model. Increasing the radial layers with fixed number of conductors and slot dimensions decreases the radial thickness and increases the circumferential thickness of the conductors. Although the conductor area is the same in both the cases, the FE and SD models with the lower radial thickness have lower errors (blue dots and crosses). This is because the variation of the induced eddy current density majorly varies along the radial direction within the conductors. Conductors with lower radial thickness would have lower current density variation, and so lower copper loss would be calculated as compared to the models with the higher radial conductor thickness.

Another important observation to highlight is the difference between the SD and the FE models featuring the same conductor arrangement. The difference between the models with 16 radial layers (blue crosses and dots) is 45% at 10 kHz, whereas the difference between the models with 12 radial layers (red crosses and dots) at the same frequency is 114.8%. This proves that the error of the SD model due to neglecting the eddy current reaction increases with the increase in the radial thickness of the conductors.

Considering all the above, it is evident that modelling the slot conductors with their actual thickness can improve the accuracy of the model as

- it can eliminate the loss overestimation due to the eddy current density over the extended conductor area;
- it can minimise the error of the SD model due to the eddy current reaction.

The next section will therefore aim at proposing an upgraded SD model which takes the actual conductor section and fill factor into account. At the authors' knowledge, this methodology has never been implemented within the SD model. This is also due to the fact that this modelling technique has always been used to estimate the copper losses below 1 kHz. Above this level, in fact, the eddy current reaction concept explained above starts to be evident and updates of the model are then necessary.

## IV. PROPOSED UPGRADE ON SD MODELLING

### A. Permeability correction

The improved SD model consists of reducing the slot area and to make it the same as the actual total conductor area within the slot. This is illustrated in Fig. 8 where the slot considered in the conventional SD model (see Fig. 8(a)) is reduced in the proposed SD model (see Fig. 8(b)). In particular, the slot is subdivided in such a way to have all the conductors with the same area. The radial and circumferential thickness of the conductors were kept approximately equal to the diameter of the actual conductors.

Reducing the slot area would however reduce the reluctance for the leakage flux in the slot. This would give a higher leakage flux in the slot which would affect the accuracy of the copper loss calculations. In order to compensate for this, the permeability for the slot SD is reduced. Since the leakage flux passes across the slot width as illustrated in Fig. 8, the permeability is reduced by the same factor  $q$  by which the slot

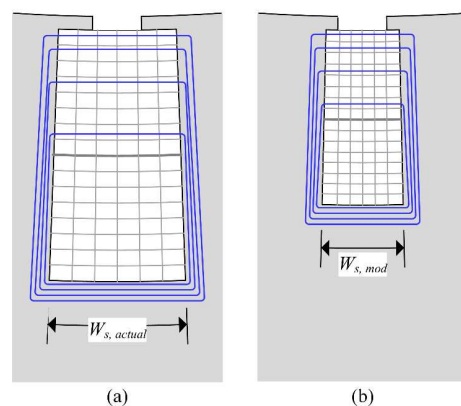


Fig. 8. Slot dimensions modification for the proposed SD methodology.

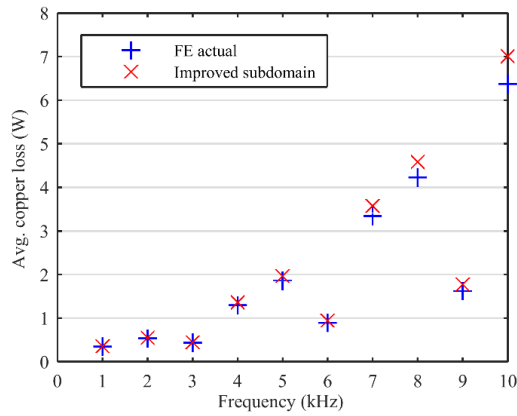


Fig. 9. Comparison between the improved SD model and the FE model.

width is reduced, as explained by (22) and (23). This maintains the original reluctance in the slot for the leakage flux.

$$q = \frac{W_{s,new}}{W_{s,actual}} \quad (22)$$

$$\mu_{slot,new} = q\mu_o \quad (23)$$

This new permeability value is used in (8) and (9), thus using the same methodology of the original SD modelling.

### B. Accuracy Comparison

The copper loss calculation results from the proposed SD model were compared with that of the actual SG's FE model. The copper loss results were obtained by exciting the windings at different frequencies, as done in section III.

The comparison between the updated SD model and the actual SG's single-slot FE model is shown in Fig. 9, where it can be observed that a drastic improvement in the accuracy of the SD model is achieved for calculating HF copper loss for round conductors. This proves the validity of the proposed model even at relatively HFs.

## V. CONCLUSION

The presented analysis investigates the accuracy of the SD model. The modelling of the true area and thickness of the conductors is shown to be critically important for the HF copper loss calculation of SGs. This is especially important for frequencies above 1 kHz. The proposed modification in the SD model has drastically improved the accuracy of the classical SD technique. Hence, it broadens the frequency spectrum to which this technique can be applied for HF copper loss analysis. The case study presented in this particular paper demonstrates its accuracy till 10 kHz. It is a fast and convenient analytical modelling technique which can be useful for analysing the effects of rapidly increasing HF switching power electronic loads on efficiency of SGs. Moreover, it can also be a useful design analysis tool for variable speed and high-speed motors which also have very HF currents flowing through their windings.

## REFERENCES

- [1] A. J. Alves, M. Wu, L. M. Neto, W. P. Calixto, and B. Alvarenga, "Modeling validation of Salient Pole Synchronous Machines from experimental inductances," in *2011 10th International Conference on Environment and Electrical Engineering*, 2011, pp. 1-4.
- [2] A. H. Samra and K. M. Islam, "Harmonic effects on synchronous generators voltage regulation," in *Southeastcon '95. Visualize the Future., Proceedings., IEEE*, 1995, pp. 376-380.
- [3] J. Q. Wang, P. C. Song, C. H. Cui, J. K. Li, and T. Yang, "Analysis of Operation of Synchronous Generator under the Distortion of Harmonic Current," in *2012 Asia-Pacific Power and Energy Engineering Conference*, 2012, pp. 1-4.
- [4] M. F. Iacchetti, G. D. Marques, J. Apsley, and S. Djurovic, "Minimum-loss operation of a variable-speed wound-field synchronous generator," in *8th IET International Conference on Power Electronics, Machines and Drives (PEMD 2016)*, 2016, pp. 1-6.
- [5] C. Liuchen, W. Qincy, and S. Pinggang, "Application of finite element method in design of a 50 kW direct drive synchronous generator for variable speed wind turbines," in *The 4th International Power Electronics and Motion Control Conference, 2004. IPEMC 2004., 2004*, vol. 2, pp. 591-596 Vol.2.
- [6] I. Jadric, D. Borojevic, and M. Jadric, "Modeling and control of a synchronous generator with an active DC load," *IEEE Transactions on Power Electronics*, vol. 15, no. 2, pp. 303-311, 2000.
- [7] S. Nuzzo *et al.*, "A Methodology to Remove Stator Skew in Small-Medium Size Synchronous Generators via Innovative Damper Cage Designs," *IEEE Transactions on Industrial Electronics*, vol. 66, no. 6, pp. 4296-4307, 2019.
- [8] A. H. M. Abu-Jalala, T. Cox, C. Gerada, M. Rashed, T. Hamiti, and N. Brown, "Power Quality Improvement of Synchronous Generators Using an Active Power Filter," *IEEE Transactions on Industry Applications*, pp. 1-1, 2018.
- [9] S. Nuzzo, P. Bolognesi, M. Galea, and D. Barater, "An Improved Automatic Voltage Regulator for Self-Excited, Small-to-Medium Power Generating Sets equipped with Brushless Excitation Systems," in *IECON 2019 - 45th Annual Conference of the IEEE Industrial Electronics Society*, 2019, vol. 1, pp. 904-909.
- [10] D. Fallows, S. Nuzzo, A. Costabeber, and M. Galea, "Harmonic reduction methods for electrical generation: a review," *IET Generation, Transmission & Distribution*, vol. 12, no. 13, pp. 3107-3113, 2018.
- [11] A. H. Abu-Jalala, T. Cox, C. Gerada, M. Rashed, T. Hamiti, and N. Brown, "Performance improvement of simplified synchronous generators using an active power filter," in *2017 IEEE Energy Conversion Congress and Exposition (ECCE)*, 2017, pp. 1845-1849.
- [12] Q. H. Quadri, S. Nuzzo, M. Rashed, C. Gerada, and M. Galea, "Modeling of Classical Synchronous Generators Using Size-Efficient Lookup Tables With Skewing Effect," *IEEE Access*, vol. 7, pp. 174551-174561, 2019.
- [13] P. A. Hargreaves, B. C. Mecrow, and R. Hall, "Open circuit voltage distortion in salient pole synchronous generators with damper windings," in *5th IET International Conference on Power Electronics, Machines and Drives (PEMD 2010)*, 2010, pp. 1-6.
- [14] S. Nuzzo, M. Degano, M. Galea, C. Gerada, D. Gerada, and N. Brown, "Improved Damper Cage Design for Salient-Pole Synchronous Generators," *IEEE Transactions on Industrial Electronics*, vol. 64, no. 3, pp. 1958-1970, 2017.
- [15] T. Lubin, S. Mezani, and A. Rezzoug, "2-D Exact Analytical Model for Surface-Mounted Permanent-Magnet Motors With Semi-Closed Slots," *IEEE Transactions on Magnetics*, vol. 47, no. 2, pp. 479-492, 2011.
- [16] L. J. Wu, Z. Q. Zhu, D. Staton, M. Popescu, and D. Hawkins, "Analytical prediction of electromagnetic performance of surface-mounted PM machines based on subdomain model accounting for tooth-tips," *IET Electric Power Applications*, vol. 5, no. 7, pp. 597-609, 2011.
- [17] T. Lubin, S. Mezani, and A. Rezzoug, "Analytic Calculation of Eddy Currents in the Slots of Electrical Machines: Application to Cage Rotor Induction Motors," *IEEE Transactions on Magnetics*, vol. 47, no. 11, pp. 4650-4659, 2011.
- [18] L. J. Wu, Z. Q. Zhu, D. Staton, M. Popescu, and D. Hawkins, "Analytical Model of Eddy Current Loss in Windings of Permanent-Magnet Machines Accounting for Load," *IEEE Transactions on Magnetics*, vol. 48, no. 7, pp. 2138-2151, 2012.
- [19] P. Arumugam, T. Hamiti, and C. Gerada, "Estimation of Eddy Current Loss in Semi-Closed Slot Vertical Conductor Permanent Magnet Synchronous Machines Considering Eddy Current Reaction Effect," *IEEE Transactions on Magnetics*, vol. 49, no. 10, pp. 5326-5335, 2013.